

A Virtual Laboratory Based on Full-Field Crystal Plasticity Simulations to Predict the Anisotropic Mechanical Properties of Advanced High Strength Steels



Haiming Zhang, Qian Li, Dongkai Xu, and Zhenshan Cui

Abstract Advanced high strength steels are of growing interest in automotive industry for their superior strength-to-weight ratio. The heterogeneous microstructure renders their complex anisotropic properties. In this work, a series of uniaxial tension (combining with the 3D digital image correlation technique) were employed to capture the plastic anisotropy of a DP980 sheet. Postmortem EBSD characterizations and the state-of-the-art full-field crystal plasticity simulations were performed to explore the effect of texture evolution and heterogeneous microstructure on its anisotropic behavior. The results indicate that the r -value of the DP980 sheet is significantly affected by the deformation level; it increases initially, and then falls continuously after localization. Specially, the r -value of the studied steel is much smaller compared to that of single-phase steels. The inhomogeneous deformation and interactions between the ferrite and martensite phases are demonstrated to account for the anisotropic behaviors of the studied material.

Keywords Anisotropy · r -value · Crystal plasticity

Introduction

Due to their excellent strength-to-weight ratio, advanced high strength steels (AHSSs) have been in great demand in automotive industry. Among them, dual-phase (DP) steel is of significant interest for its simultaneous good formability and high strength and used to produce critical parts like B-pillar and engine cradle, etc. [1] Nevertheless, the heterogeneous multi-phase microstructure of AHSSs also leads to their complex mechanical properties [2]. AHSSs sheets essentially show

H. Zhang (✉) · Q. Li · Z. Cui

School of Materials Science and Engineering, Shanghai Jiao Tong University, 1954 Huashan Road, Shanghai 200030, PR China
e-mail: hm.zhang@sjtu.edu.cn

D. Xu

Research Institute, Baoshan Iron and Steel Co., Ltd., State Key Laboratory of Development and Application Technology of Automotive Steels (BaoSteel), Fujin Road 655, Shanghai 201900, China

distinct mechanical anisotropy due to the preferential orientation (i.e., crystallographic texture) developed in the proceeding thermomechanical operations. The typical texture component γ fiber ($\langle 111 \rangle \parallel \text{ND}$, with ND represents the normal direction of sheet) of body-centered cubic (BCC) metals generally improves the deep drawing ability; while the α fiber ($\langle 110 \rangle \parallel \text{RD}$, with RD represents the rolling direction) does the opposite.

A critical parameter used to characterize the plastic anisotropy is the Lankford coefficient (r -value) from uniaxial tension of metal sheets. Since the deep drawing ability of metal sheets generally relates to r -values which are easily accessible through uniaxial tension, r -values therefore are frequently used for calibration of yield functions, for instance, Hill48 [3] and Yld2004 [4] criteria, etc. As a first-hand and important parameter of polycrystalline sheets, r -values of single-phase BCC steels have been extensively investigated by many researchers, for instance, 1.64–2.43 for IF steel [5], 1.4–1.8 for low-carbon steel [6] and 1.2–1.8 for ferrite stainless steel [7]. For AHSSs, however, r -values were announced to be 0.85–1.1 [8, 9], i.e., much smaller than those of single-phase steels. Unlike the single-phase body-centered cubic (BCC) steels, the anisotropic behavior of multi-phases steels is not well understood yet.

Crystal plasticity (CP) modeling is an effective and commonly used approach for studying the anisotropic behaviors and underneath micro-mechanisms of polycrystalline metals. Using a CPFEM scheme, Woo et al. [10] verified that the crystal orientations of ferrite phase have a great influence on the strain localization and void initiation in the ferrite matrix near the phase boundaries for a DP980 steel sheet. Based on a full-field CPFEM framework, Pagenkopf et al. [11] revealed the relation between the martensite morphology and the flow stress as well as the r -values. Zhang et al. [12] developed a virtual laboratory based on high-resolved CP modeling to predicted the anisotropy of aluminum alloys, and the predicted yield stress points were adopted to identify advanced yield functions successfully.

In this work, we adopt microstructure-based full-field crystal plasticity (CP) simulations as a virtual laboratory to predict the plasticity anisotropy of a cold-rolled AHSS (DP980), and further to probe the micromechanical behaviors due to the heterogeneous microstructure. The results are verified and explained complementally via a series of uniaxial tension (combining with the 3D digital image correlation technique) as well as postmortem EBSD characterizations.

Experiments and Full-Field Crystal Plasticity Modelling

Uniaxial Tensile Tests and Post-Mortem EBSD Characterizations

The studied material is a commercial cold-rolled DP980 sheet of 1.2 mm thickness (provided by Baosteel). To explore the mechanical anisotropy of the sheet, uniaxial

tensile tests along seven directions (i.e., 0° , 15° , 30° , 45° , 60° , 75° , and 90° to the RD) were performed on the specimens via an electronic testing machine (Instron Model 8080 with a load cell of 100KN). The crosshead velocity is 3 mm/min. The gauge length and width of the dog-bone specimens are 50 mm and 12.5 mm, respectively. A 3D DIC system (Aramis) was used to capture the strain field evolution up to fracture.

To investigate the influence of texture evolution on mechanical anisotropy, the microstructures before and after uniaxial tensile tests were characterized using a VEGA 3 field emission SEM equipped with an Oxford EBSD detector at 20 kV. The initial and deformed specimens were ground with 100, 240, 320, and 600 grit SiC papers respectively, and then polished with $9\ \mu\text{m}$ and $3\ \mu\text{m}$ diamond suspensions, followed by $0.05\ \mu\text{m}$ alumina suspension. Finally, the specimens were vibratory polished with $0.02\ \mu\text{m}$ silica suspension for two hours. For the deformed specimens, the region of interest is on the RD-TD plane and close to the fracture surface, where the material has undergone larger deformation.

Microstructure-Based Full-Field Crystal Plasticity Modelling

To investigate the influence of the heterogeneous microstructure on the anisotropic behaviors, microstructure-based full-field CP simulations were performed on the DP980 sheet. The plastic velocity gradient resulted from dislocation slip is written as

$$\mathbf{L}^P = \sum_{\alpha} \dot{\gamma}^{\alpha} \mathbf{S}^{\alpha} \quad (1)$$

Here, \mathbf{S}^{α} and $\dot{\gamma}^{\alpha}$ are the Schmid tensor and the slip rate of the α slip system respectively.

A phenomenological rate-dependent constitutive model was adopted to describe the slip rate resulting from dislocation slip. It is expressed as

$$\dot{\gamma}^{\alpha} = \dot{\gamma}_0 \left| \frac{\tau^{\alpha}}{g^{\alpha}} \right|^{1/m} \text{sign}(\tau^{\alpha}) \quad (2)$$

Here, $\dot{\gamma}_0$ denotes the reference slip rate, m refers to the rate sensitivity coefficient, and g^{α} refers to the slip resistance. The evolution of g^{α} is formulated as

$$\begin{cases} \dot{g}^{\alpha} = \sum_{\beta} h_{\alpha\beta} \dot{\gamma}^{\beta} \\ h_{\alpha\beta} = h_0 [q + (1 - q) \delta^{\alpha\beta}] \left| 1 - \frac{g^{\beta}}{g_{\infty}^{\beta}} \right|^a \end{cases} \quad (3)$$

Here, h_0 is the initial hardening modulus of slip systems, g_{∞} is the saturated slip resistance, a is an estimated constant, and q refers to the hardening coefficient describing

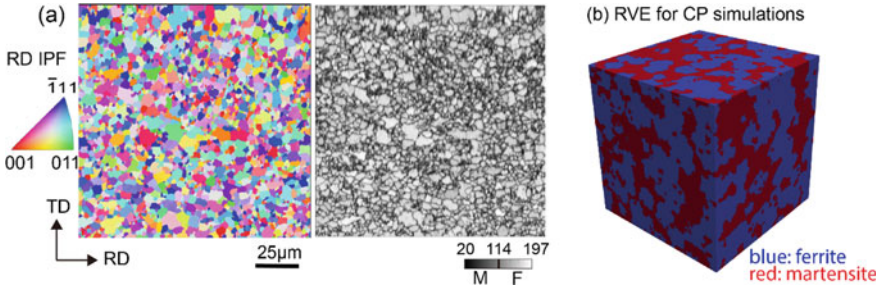


Fig. 1 a Microstructure of the as-received DP980 sheet: orientation imaging microscopy and band contrast maps obtained by EBSD; the 3D-RVE reconstructed by DREAM. 3D based on the EBSD data

the interaction between slip systems. $q = 1.0$ for coplanar interaction and 1.4 for non-coplanar interaction.

In this work, the CP constitutive model considers $\{\bar{1}10\}\langle 111 \rangle$ and $\{\bar{2}11\}\langle 111 \rangle$ slip for both ferrite and martensite phases. As shown in Fig. 1a, EBSD data of the initial microstructure was used to separate the ferrite and martensite phases based on the band contrast (BC) value. After that, 3D representative volume elements were reconstructed via an open-source software DREAM.3D with emphasizing of matching phase constituent and orientations; the RVE is exemplified in Fig. 1b. A genetic algorithm-based inverse method then was adopted to identify the CP material parameters for both ferrite and martensite phases. The constitutive parameters for the studied DP980 sheet are listed in Table 1. The methodology was validated by comparing the predicted flow stress curves with the experimental ones from uniaxial tensile tests. The full-field CP simulations were conducted in the open-source spectral method solver DAMASK. Periodic boundary condition was applied on the RVEs to simulate uniaxial tension along different directions. More details can be found in Li et al. [13].

Results and Discussion

Figure 2 displays the contour maps of the equivalent plastic strain $\bar{\epsilon}^p$ for uniaxial tensile specimens at different stages. As can be seen from Fig. 2a, the strains of the specimens are well distributed at the stage of $\bar{\epsilon}^p = 5.5\%$ except for 60° and 75° specimens, which manifest moderate strain localizations. With deformation, the strain localizations get more obvious. At the stage before fracture shown in Fig. 2b, shear bands with angle of 50° – 55° to the loading direction can be observed in all the specimens. The results demonstrate that the DIC technique used in this work provides a high-fidelity strain field during the entire uniaxial tension process.

The Lankford coefficient (r -value), defined as the ratio of the width to thickness plastic strain rates ($\dot{\epsilon}_w^p/\dot{\epsilon}_t^p$), is a critical parameter for characterizing the plastic

Table 1 The constitutive parameters of the CP model for the DP980 steel

Phase	System	g_0/MPa	g_∞/MPa	h_0/GPa	a	m	$\dot{\gamma}_0/s^{-1}$	C_{11}/GPa	C_{12}/GPa	C_{44}/GPa
Ferrite	$\{\bar{1}10\}\langle 111 \rangle$	150.8	223.4	2.0	1.9	0.05	0.001	233.3	135.5	118.0
	$\{\bar{2}11\}\langle 111 \rangle$	154.0	614.3							
Martensite	$\{\bar{1}10\}\langle 111 \rangle$	644.3	917.8	1.12	1.9	0.05	0.001	417.4	242.4	211.1
	$\{\bar{2}11\}\langle 111 \rangle$	725.2	1021.2							

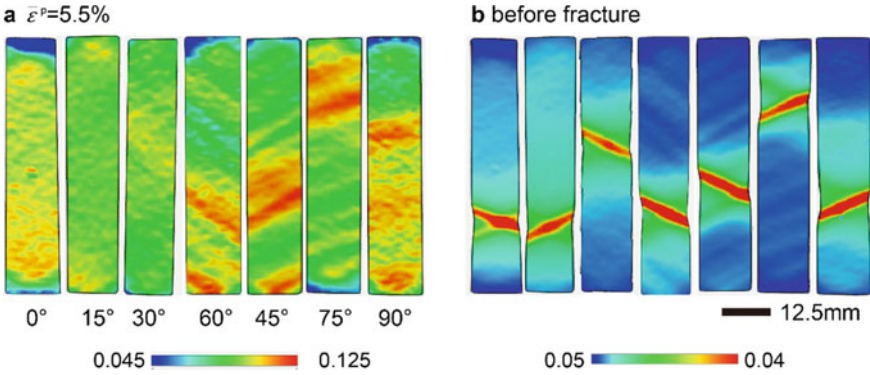


Fig. 2 The contour maps of equivalent plastic strain $\bar{\epsilon}^p$: **a** at global $\bar{\epsilon}^p = 5.5\%$, **b** at global $\bar{\epsilon}^p = 9\%$

anisotropy of metal sheets. Figure 3 presents the evolution of r -value for the specimens tensioned along the seven directions. As can be seen, the r -value of the studied DP980 sheet is highly sensitive to the loading directions. For instance, the large value appears in the diagonal direction (DD) specimen and the lowest one in the RD specimen. Different from the traditional low-carbon steels whose r -values generally exceeding 2.0, in most cases the r -values of the studied DP980 sheet are below 1.0. This suggests that the DP980 sheet is more vulnerable to reduction in thickness than width. As illustrated in Fig. 3, the r -value also relies on the strain level. For all the specimens, the r -values ascends gradually with deformation initially and then decrease until failure. The inflection point arises near global $\bar{\epsilon}^p = 0.055$, taking the smallest value for 75° specimen and largest for 0° and 15° specimen. Associated with the strain distribution at $\bar{\epsilon}^p = 5.5\%$ shown in Fig. 2a, it is concluded that the heterogeneous deformation resulting from strain localization mainly accounts for the transition of r -values. Furthermore, the results suggest that the traditional practice

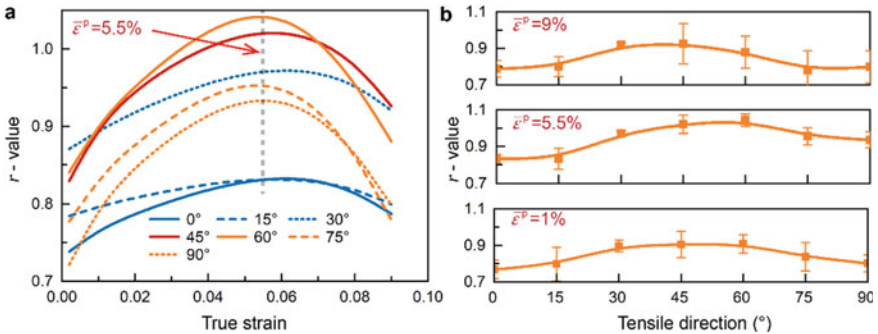


Fig. 3 **a** The evolution of r -values with deformation, **b** the variation of r -values with respect to the loading directions at strain levels of $\bar{\epsilon}^p = 1\%$, 5.5% and 9%

of using the r -values at a specific stage to characterizing the plastic anisotropy and calibrating yield functions simplifies the anisotropy evolution of AHSS sheets.

Figure 4 shows the ND IPF and RD IPF reconstructed with the MATLAB toolbox MTEX for specimens tensioned along RD, DD, and TD. Significant texture change from main component $\{111\}\langle 11\bar{2}\rangle$ to $\{111\}\langle 011\rangle$ is clearly observed in all the specimens, especially for the DD specimen, which agrees with the uniaxial tensile experiments as the DD specimen has the largest r -value in all the three specimens. After deformation, the orientations spread from $[011]$ to $[\bar{1}12]$ and gather at the pole $[\bar{1}11]$, leading to the preservation of γ fiber and weakening of α fiber. This texture evolution is inferred to account for the gradual ascent for r -values of the studied DP980 sheet before strain localization since the γ fiber generally improves r -values of polycrystalline sheets while the α fiber does the opposite.

Figure 5 presents the comparison between the predicted and experimental r -values of the studied DP980 sheet with respect to loading directions obtained from CP simulations. Despite the mild deviation, the evolution of r -values suggests that the CP modeling successfully forecasts the in-plane anisotropy of r -values. Furthermore, referring to the 0° and 90° specimens whose simulated r -values matched very well with the experimental ones. It is verified that the CP modeling is more precise when the principal axes of stress coincide with that of the material. Previous work of Zhang et al. [12] on an AA3104 aluminum sheet demonstrated the nice dependability of full-field CP based virtual laboratory in modeling the plastic anisotropy of single-phase metals. Figure 5 further proves that the CP modeling with high-resolution is promising in predicting the anisotropy of multi-phase polycrystalline metals.

To investigate the influence of heterogeneous microstructure on anisotropic properties, contour maps of equivalent strain and r -value at the stage of global $\bar{\epsilon}^p = 0.09$

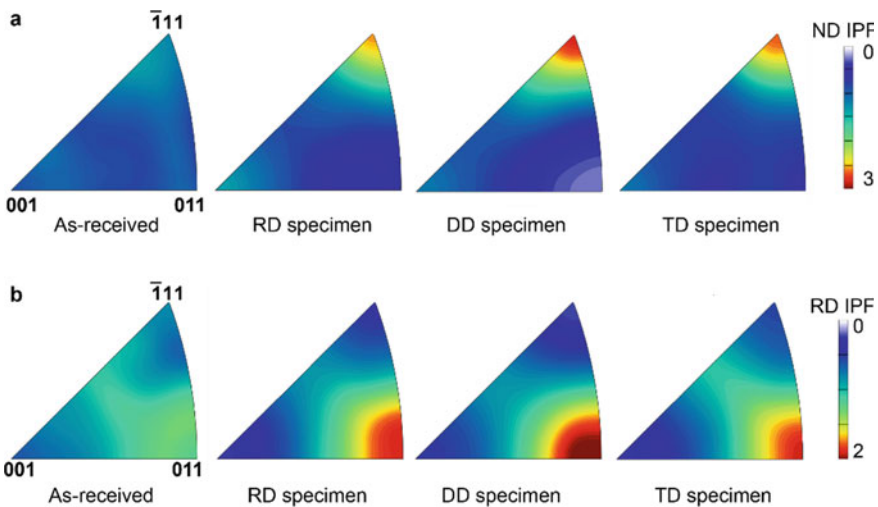
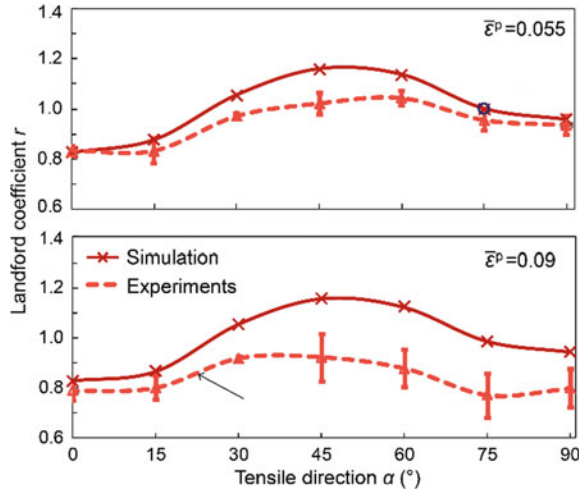


Fig. 4 a The ND IPF; b the RD IPF of specimens tensioned along RD, DD, and TD

Fig. 5 a The in-plane anisotropy of r -values predicted by CP simulations at strain levels of $\bar{\epsilon}^p=5.5\%$ and 9%



are studied for the RD, DD, and TD specimens, as shown in Fig. 6. As anticipated, the grain-level strain distributions of all the specimens are strongly inhomogeneous; strain localizations mainly occur in the phase boundaries (PBs) and in the necklaces of the martensite islands. The soft ferrite matrix underwent a larger deformation than the hard martensite islands, and local shear bands with direction consistent to the macroscopic shear bands shown in Fig. 2b are clearly observed near the PBs. That is, the soft ferrite matrix accommodates the imposed deformation while the hard martensite phase maintains deformation compatibility. The deformation constraint resulting from the PBs of the heterogeneous microstructure dominates the strain distribution of the specimens and could reduce the overall r -values of the DP steels [13]. Figure 6a further demonstrates that the three RVEs show a quite similar distribution of strain, i.e., the grain-level deformation partition is more influenced by the heterogeneous microstructure while less by the loading direction.

Regarding the contour map of r -values, as shown in Fig. 6b, the distributions are also highly inhomogeneous. For RVEs tensioned along different directions, they all have r -values smaller than 0.5 for most areas, especially for the RVEs tensioned in RD and TD. According to the statistics, the proportion of material points with r -value below 0.45 is 36.9% for the RD RVE and 33.9% for the TD RVE, which is much larger than that of the DD RVE (26.2%). The result is consistent with Fig. 3b, as the DD specimen has a higher r -value compared to the RD and TD specimens, which further proves the reliability of CP simulation in modeling multi-phase polycrystalline. Unlike the distribution of strain, Fig. 6b shows that the grain-level r -value is more affected by the loading direction.

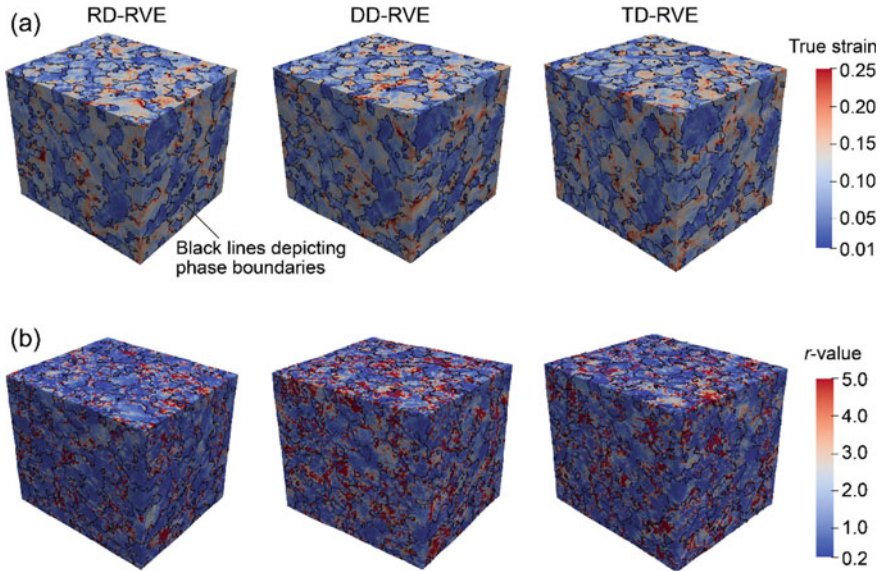


Fig. 6 The contour maps of **a** true strain and **b** r -values at the stage of global $\bar{\epsilon}^p = 0.09$ simulated by full-field CP-based virtual laboratory for the RD, DD, and TD specimens

Conclusions

A series of uniaxial tensile tests and postmortem EBSD characterizations combining with the full-field CP simulations were conducted to explore the anisotropic behaviors of the DP980 steel sheet and the influence of the heterogeneous microstructure. The mechanical anisotropy and the evolution of r -value were evidenced with the 3D DIC technique. The results indicate that the texture evolution, strain localization, and plastic heterogeneity resulting from the dual-phase heterogeneous microstructure dominates the r -values jointly. The texture evolution from $\{111\}\langle 11\bar{2}\rangle$ to $\{111\}\langle 011\rangle$ intensifies the γ fiber and weakens the α fiber, leading to the gradual ascent of r -values at the beginning. Afterwards, the strain localization brings down the thinning resistance of the sheet and brings about the continuous fall of r -values. The high-resolved CP simulations successfully reproduce the evolution of r -values with respect to tensile directions and demonstrate the influence of the heterogeneous microstructure on r -values. The heterogeneous deformation between the ferrite and martensite phases results in strain partition and deformation constraint. Such deformation constraint is confirmed to reduce the overall r -values of the DP980 sheet. The grain-level distributions of strain and r -values show that the strain partition is more affected by the heterogeneous microstructure, while r -values show strongly dependence on loading directions.

Acknowledgements The authors acknowledge the funding support from the National Natural Science Foundation of China with the project No. 52075329 and Shanghai Rising-Star Program (20QA1405300).

References

1. Stuart K, Menachem K (2014) Advanced high-strength steels: application guidelines version 5.0, WorldAutoSteel
2. Cai Z, Diao K, Wu X, Wan M (2016) Constitutive modeling of evolving plasticity in high strength steel sheets. *Int J Mech Sci* 43–57
3. Hill R, Orowan E (1948) Mathematical and physical sciences. *Math Phys Sci* 193:281–297
4. Barlat F, Aretz H, Yoon JW, Karabin ME, Brem JC, Dick RE (2005) Linear transformation based anisotropic yield functions. *Int J Plast* 5:1009–1039
5. Oh GJ, Lee KM, Huh MY, Park JE, Park SH, Engler O (2017) Effect of r-value and texture on plastic deformation and necking behavior in interstitial-free steel sheets. *Met Mater Int* 1:26–34
6. Tada M, Nakagawa Y, Kojima K (2018) Effect of annealing temperature and coiling temperature on r-value of Nb and B-added extra low-carbon steel. *ISI J Int* 5:970–977
7. Yazawa Y, Muraki M, Kato Y, Furukimi O (2003) Effect of chromium content on relationship between r-value and 111 recrystallization texture in ferritic steel. *ISI J Int* 10:1647–1651
8. Panich S, Barlat F, Uthaisangsuk V, Suranuntchai S, Jirathearanat S (2013) Experimental and theoretical formability analysis using strain and stress based forming limit diagram for advanced high strength steels. *Mater Des* 756–766
9. Huh J, Huh H, Lee CS (2013) Effect of strain rate on plastic anisotropy of advanced high strength steel sheets. *Int J Plast* 23–46
10. Woo W, Em V, Kim EY, Han SH, Han YS, Choi SH (2012) Stress–strain relationship between ferrite and martensite in a dual-phase steel studied by in situ neutron diffraction and crystal plasticity theories. *Acta Mater* 20:6972–6981
11. Pagenkopf J, Butz A, Wenk M, Helm D (2016) Virtual testing of dual-phase steels: Effect of martensite morphology on plastic flow behavior. *Mater Sci Eng A* 672–686
12. Zhang H, Diehl M, Roters F, Raabe D (2016) A virtual laboratory using high resolution crystal plasticity simulations to determine the initial yield surface for sheet metal forming operations. *Int J Plast* 111–138
13. Li Q, Zhang H, Chen F, Xu D, Sui D, Cui Z. Study on the plastic anisotropy of advanced high strength steel sheet: experiments and microstructure-based crystal plasticity modelling. *Int J Mech Sci*